

Soft X-ray absorption spectroscopy and resonant inelastic X-ray scattering spectroscopy below 100 eV: probing first-row transition-metal *M*-edges in chemical complexes

Hongxin Wang,^{a,b*} Anthony T. Young,^c Jinghua Guo,^c Stephen P. Cramer,^{a,b} Stephan Friedrich,^d Artur Braun^e and Weiwei Gu^b

^aDepartment of Chemistry, University of California, 1 Shields Avenue, Davis, CA 95616, USA,

^bPhysical Biosciences Division, Lawrence Berkeley National Laboratory, 1 Cyclotron Road, Berkeley, CA 94720, USA, ^cAdvanced Light Source, Lawrence Berkeley National Laboratory, 1 Cyclotron Road, Berkeley, CA 94720, USA, ^dAdvanced Detector Group, Lawrence Livermore National Laboratory, 7000 East Avenue, Livermore, CA 94550, USA, and ^eLaboratory for High Performance Ceramics, Empa, Swiss Federal Laboratories for Materials Science and Technology, CH-8600 Dübendorf, Switzerland. E-mail: hxwang2@lbl.gov

X-ray absorption and scattering spectroscopies involving the 3*d* transition-metal *K*- and *L*-edges have a long history in studying inorganic and bioinorganic molecules. However, there have been very few studies using the *M*-edges, which are below 100 eV. Synchrotron-based X-ray sources can have higher energy resolution at *M*-edges. *M*-edge X-ray absorption spectroscopy (XAS) and resonant inelastic X-ray scattering (RIXS) could therefore provide complementary information to *K*- and *L*-edge spectroscopies. In this study, *M*_{2,3}-edge XAS on several Co, Ni and Cu complexes are measured and their spectral information, such as chemical shifts and covalency effects, are analyzed and discussed. In addition, *M*_{2,3}-edge RIXS on NiO, NiF₂ and two other covalent complexes have been performed and different *d*-*d* transition patterns have been observed. Although still preliminary, this work on 3*d* metal complexes demonstrates the potential to use *M*-edge XAS and RIXS on more complicated 3*d* metal complexes in the future. The potential for using high-sensitivity and high-resolution superconducting tunnel junction X-ray detectors below 100 eV is also illustrated and discussed.

Keywords: 3*d* metal *M*-edge; soft X-ray absorption spectroscopy (XAS); resonance inelastic X-ray scattering (RIXS); superconducting tunnel junction (STJ) X-ray detector.

1. Introduction

First-row (3*d*) transition-metal complexes are of wide importance in inorganic and bioinorganic chemistry (Lancaster, 1988). Their *K*-edge (4–10 keV) and *L*-edge (400–1000 eV) X-ray absorption spectra have been studied and reported in a variety of applications (Ohzuku & Makimura, 2006; Waddill *et al.*, 1998; van der Laan & Kirkman, 1992; Okada & Kotani, 1992; Wang *et al.*, 1998, 2000). Owing to the higher energy resolution ($\Delta E \simeq 0.2$ eV *versus* ~ 1 eV) and the stronger $2p \rightarrow 3d$ interaction, *L*-edge X-ray absorption spectroscopy (XAS) has distinct advantages for resolving detailed electronic configurations (Wang *et al.*, 2000; van der Laan & Kirkman, 1992; Okada & Kotani, 1992; Waddill *et al.*, 1998), while *K*-edge XAS is typically used to measure geometric structures and chemical shifts.

The first transition metal *M*-edges correspond to $3p \rightarrow 3d$ transitions that fall in the energy region below 100 eV, *e.g.* Fe (*M*₃) at 52.7 eV, Co at 59.9 eV, Ni at 66.2 eV, Cu at 75.1 eV and Zn at 88.6 eV. Analogous to *L*-edge XAS, *M*-edge XAS is also useful in obtaining orbital and electronic information owing to the strong interaction between 3*p* and 3*d* orbitals, and could provide different chemical information complementary to the *K*-edges and *L*-edges. In addition, higher energy resolution in this low-energy region is straightforward to obtain experimentally (Young *et al.*, 1999). Unfortunately, 3*d* metal *M*-edge XAS below 100 eV is less frequently reported (Branchard *et al.*, 2008; Koide *et al.*, 1991). On the other hand, *M*-edge resonance inelastic X-ray scattering (RIXS) (Kuiper *et al.*, 1998; Chiuzaibaian *et al.*, 2005, 2008) as well as electron energy-loss spectroscopy (Steiner *et al.*, 1996) have been reported in several publications, paving the way

to an improved understanding of 3d metal *M*-edge spectroscopy.

In this publication, we examined the $M_{2,3}$ -edge XAS and $M_{2,3}$ -edge RIXS for several 3d metal complexes. The preliminary results on these complexes will serve as the first step to further motivate studies on more complicated and biologically relevant complexes in the future.

2. Experiments

Powder samples of NiF₂, NiCl₂, NiBr₂, NiI₂, NiO, Ni(OH)₂, LiNiO₂, CoF₂ and CuO were evaluated by *M*-edge XAS at energies from 50 to 100 eV. LiNiO₂ was synthesized by a high-temperature combustion method (Rao *et al.*, 2001) at Argonne National Laboratory, USA. All other samples were purchased from Sigma-Aldrich (purity = 98.5%–99.5%) and used without further purification. Although these materials are nominally not air-sensitive, all samples were still prepared in a nitrogen-filled glovebox as a precaution. Powder samples of NiO, NiF₂, (Ph₄As)₂Ni^{II}[S₂C₂(CF₃)₂]₂ and ("Bu₄N)Ni^{III}[S₂C₂(CF₃)₂]₂ {[Ni(II)(tfd)₂]⁺ and [Ni(III)(tfd)₂]⁻, respectively, for short} were measured by Ni $M_{2,3}$ -edge RIXS. The two Ni dithiolene complexes were synthesized at the ExxonMobil Research Co. For each experiment, sample powders were ground fine and attached to a copper sample holder using UHV-compatible double-sided carbon tape. The samples were prepared and sealed in a glovebox and transferred into the UHV measurement chamber using a load lock.

The 3d metal *M*-edge XAS spectra were measured at BL4.0.2 at the Advanced Light Source (ALS), USA. Its monochromator covers the energy region from 50 to 1800 eV and has a resolving power ($\Delta E/E$) of 9000 or better at energies below 100 eV (Young *et al.*, 1999). To increase the X-ray flux at these low energies, our XAS experiments were performed with the storage-ring energy at 1.5 GeV rather than at the regular 1.9 GeV. The measurement chamber was maintained at a vacuum pressure of 2×10^{-9} torr or lower, enabling windowless operation between the storage ring, samples and detector. The entrance and exit slits were both set at 40 μ m, corresponding to an energy resolution of $\Delta E \simeq 0.01$ eV.

The 3d metal *M*-edge XAS spectra were recorded in electron yield mode (I_E) (Stohr, 1992) using a Galileo 4716 channeltron electron multiplier. The incident beam intensity (I_0) was monitored *via* a gold-plated grid at the entrance of the measurement chamber, and the beamline energy was calibrated by setting the M_3 -edge of NiF₂ to the Ni ionization value of 66.2 eV (CXRO, 2000). The scans were recorded with a step size of 0.05 eV. A step size of 0.01 eV on NiF₂ did not provide a better spectral resolution. The data acquisition time was 5 s per point, and each spectrum presented here is the average of four raw scans (I_E/I_0).

The Ni $M_{2,3}$ -edge RIXS was measured at ALS BL7.0 using a 3 m grazing-incidence grating spectrograph (Kuiper *et al.*, 1998). The spectrometer's slit width of 30 μ m gave an energy resolution of 0.2 eV. The RIXS experiments were also performed at a storage ring energy of 1.5 GeV, which gave a lower photon energy limit of 60 eV for the undulator. The

energy resolution of the monochromator was set to be less than 0.05 eV for the incident photon beam energies of 66, 68 and 70 eV. The total energy resolution for the RIXS experiment was about 0.2 eV as determined by the full width at half-maximum of the elastic peak in the RIXS spectra.

3. Results and discussions

3.1. XAS analysis

Following the similar procedure developed for *L*-edge XAS (Wang *et al.*, 1998, 2000), a piecewise linear background slope was subtracted from the electron yield data I_E/I_0 below the L_3 and above the L_2 regions. The edge jump was then normalized to unity. The resulting spectra, as shown in Fig. 1(a) for NiBr₂, contain the absorption peaks from resonant $3p \rightarrow 3d$ transitions and a broad non-resonant background. Subtracting two broadened arctangent functions then produced the background-free nickel halide spectra, such as those shown in Figs. 1(b) to 1(e).

With the NiF₂ M_3 -edge being calibrated to 66.2 eV, each NiX₂ spectrum ($X = F, Cl, Br$ and I) has a resolved or partially resolved doublet at 66.2 and 67.0 eV. These features are due to the M_3 and M_2 transitions. These measured energy positions vary slightly from theoretical values of 66.2 and 68.0 eV (CXRO, 2000), possibly due to the difference in the molecular environment between elemental Ni and Ni complexes. The literature value of the binding energies in this region may also not be very accurate either, similar to the case of elemental lithium and its complexes (CXRO, 2000; Braun *et al.*, 2007).

We also measured $M_{2,3}$ -edge XAS for several other 3d metal compounds (Fig. 2a). The $M_{2,3}$ -edges of CoF₂ were measured at 58.8 and 59.8 eV, and those of CuO at 75.0 and 77.1 eV, respectively. These values are close to the theoretical electron binding energies of 58.9 and 59.9 eV for Co and 75.3

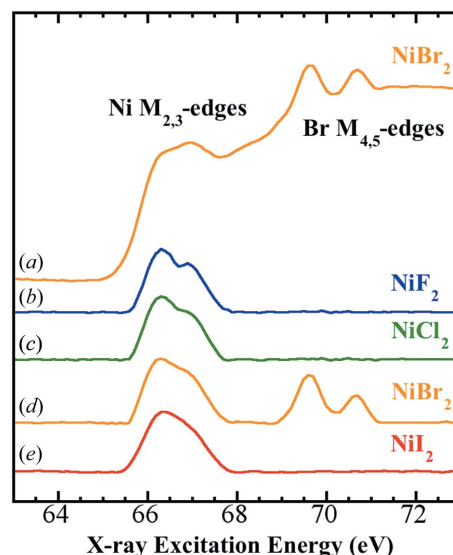


Figure 1
 $M_{2,3}$ -edge XAS spectra for several nickel halide complexes: NiBr₂ with non-resonant absorption step background (a), NiF₂ (b), NiCl₂ (c), NiBr₂ (d), NiI₂ (e) with background removed.

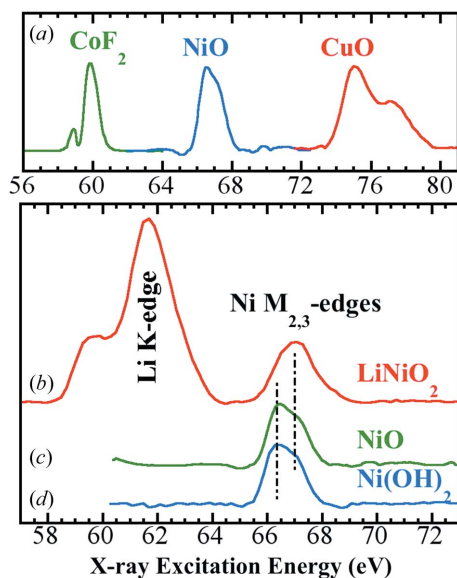


Figure 2
 $M_{2,3}$ -edge XAS of CoF_2 (a, green), NiO (a, blue) and CuO (a, red); $M_{2,3}$ -edge XAS of LiNiO_2 (b), NiO (c) and Ni(OH)_2 (d). The vertical bars are the $M_{2,3}$ -edge peak positions for LiNiO_2 and NiO .

and 77.3 eV for Cu (CXRO, 2000) as well. The overall $M_{2,3}$ -peak broadens with increasing atomic number, consistent with the larger splitting between the M_3 and M_2 energies in Cu compared with Ni and Co. While the CoF_2 spectrum has a peak width of ~ 1 eV, the CuO spectrum has peaks obviously wider than 1 eV and a wider split between M_3 and M_2 .

Besides the $3d$ metal $M_{2,3}$ -edges, there are other elements with edges in the region below 100 eV, such as the Li K -edge, Al and Si $L_{2,3}$ -edges and Se and Br $M_{4,5}$ -edges. In this study we have observed lithium K -edge XAS in LiNiO_2 (Fig. 2b), which shows two strong absorption peaks at 61.7 and 59.7 eV that are shifted from elemental Li at 63 eV and Li_3N at 66 eV (Sonntag, 1974; Braun *et al.*, 2007). We have also observed bromine $M_{4,5}$ -edge XAS in NiBr_2 with two distinct peaks at 69.6 and 70.6 eV [Figs. 1(a) and 1(d)]. These examples show that XAS below 100 eV is not limited to just probing the first-row transition-metal $M_{2,3}$ -edges.

3.2. Chemical shift and covalence

M -edge XAS spectra of Ni oxide and halide complexes were used to illustrate two of the most interesting and useful aspects in spectroscopic studies: chemical shift and covalence. The absorption-peak centroid difference between the Ni ions in NiO [or Ni(OH)_2] [Figs. 2(c) and 2(d)] and the Ni ions in LiNiO_2 [Fig. 2(b)] is found to be +0.8 eV. The charge compensation mechanism in LiNiO_2 or non-stoichiometric $\text{Li}_{1-x}\text{Ni}_{1+x}\text{O}_2$ ($0 < x < 1$) has been the subject of significant studies for over two decades (Kuiper *et al.*, 1989; Rougier *et al.*, 1995; Pickering *et al.*, 1993; Chen & Harding, 2012; Guo *et al.*, 2004; Montoro *et al.*, 1999) and the Ni in LiNiO_2 is not necessarily Ni(III). A detailed discussion on Ni(II) *versus* Ni(III) in LiNiO_2 goes beyond the scope of this study.

However, our M -edge XAS indicates that Ni in LiNiO_2 has an obviously higher absorption centroid and thus a higher valence than Ni(II). This result is consistent with the following: (i) the Ni K -edge observations for the LiNiO_2 complex (Mansour & Melendres, 1997); (ii) although previous L -edge studies claimed Ni(II) for LiNiO_2 , their spectra (VanElp *et al.*, 1992) are still different from a typical Ni(II) complex; (iii) the shift between NiO and LiNiO_2 is also comparable with the centroid shift of +0.9 eV in L_3 -edge XAS for other Ni(II) and Ni(III) complexes (Wang *et al.*, 1998).

On the other hand, NiO and Ni(OH)_2 have a very similar $M_{2,3}$ -edge XAS, including the peak positions and the overall spectral features. This is consistent with the fact that both contain a high-spin Ni(II) site and both have similar electronic and geometric structures.

Besides chemical shift, covalence is another important aspect relevant to materials' properties. As seen in Fig. 1, NiF_2 has a resolved doublet at 66.2 and 67.0 eV while NiCl_2 has a less resolved doublet at 66.2 and 67.0 eV. The spectral multiplets show a trend of less and less resolved features from NiF_2 to NiI_2 . In these chemical complexes, owing to the increase of the covalency from NiF_2 to NiI_2 , the p orbitals become more delocalized, which results in broadened Ni $3d$ orbitals owing to increased pd mixing, and therefore a less-resolved spectral multiplet. A similar trend has been observed in Ni L -edges as well, for example between NiF_2 and NiBr_2 (Cramer *et al.*, 1998).

3.3. RIXS: Ni $d-d$ transition

Besides XAS, $M_{2,3}$ -edge RIXS spectra were also evaluated for several ionic and covalent chemical complexes in this study. RIXS, also called resonant X-ray Raman (XRR) spectroscopy, is a powerful technique for studying the elementary excitations in solids and ionic complexes (Chiuzbaian *et al.*, 2005, 2008; Lee *et al.*, 2007). Using excitation energies at specific core-level thresholds, one can produce targeted excitations and determine their atomic and energetic origin. Therefore RIXS has more selectivity than XAS in probing species in materials of higher chemical or electronic complexity. In addition, XAS probes the density of states (DOS) of the unoccupied $3d$ orbitals, while RIXS measures the DOS of the occupied $3d$ orbitals; the two techniques therefore provide complementary information (Guo *et al.*, 2003; Gunnelin *et al.*, 1999).

RIXS in the soft X-ray region on a chemical complex was first studied in 1989 on Cu $d-d$ excitations for $\text{Sr}_2\text{CuO}_2\text{Cl}_2$ with a resolution of 0.2 eV (Kuiper *et al.*, 1998). Different electronic Cu $d-d$ structures, such as xy , xz , yz and $3z^2$ orbitals, were resolved and analyzed. In 2005, localized electronic excitations in NiO were studied with RIXS with a high energy resolution of 130 meV that allowed clear identification of several $d-d$ excitation features (Chiuzbaian *et al.*, 2005). For example, the $d-d$ transition peaks were observed at 1, 1.8 and 3 eV from which crystal field parameters were calculated. The RIXS spectral dependence on excitation energy also provided

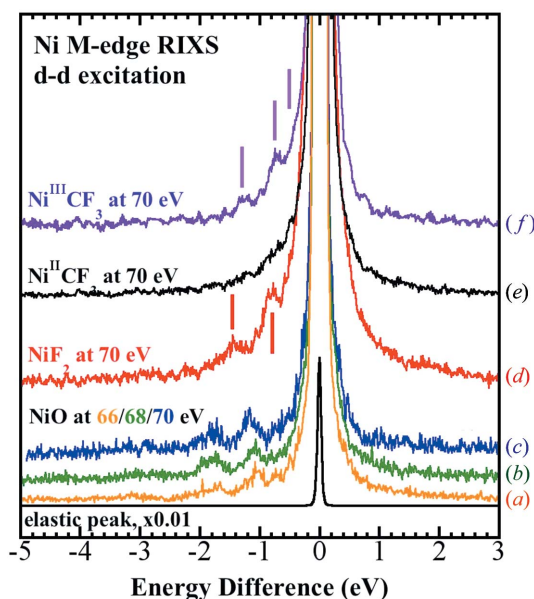


Figure 3

Observed $M_{2,3}$ -edge RIXS (energy difference spectra) of NiO, excited at 66 (a, orange), 68 (b, green), 70 eV (c, blue); and of NiF₂ (d, red), [Ni(II)(tfd)₂][−] (e, black), [Ni(III)(tfd)₂][−] (f, purple) at 70 eV. The black curve at the bottom illustrates the elastic peak position ($\times 0.01$). The vertical bars correspond to the possible d - d transition peaks.

evidence for local spin flip. These reports pave the way to understanding the $3d$ metal M -edge RIXS.

For our M -edge RIXS on NiO, there are two small but distinct peaks at about -1.1 eV and -1.8 eV, and a possible weak feature at about -3 eV when excited at 66, 68 and 70 eV [Figs. 3(a), 3(b) and 3(c)]. These peaks correspond to the d - d transitions for Ni in NiO, similar to the overall feature of the earlier Ni M -edge (Chiuzbaian *et al.*, 2005) and K -edge (van Veenendaal *et al.*, 2011) RIXS on NiO. At different excitation energies, NiO M -edge RIXS reproduces the d - d transition peaks, notwithstanding that minor differences exist. For more complex samples, different excitation energies could lead to different RIXS features, and thus RIXS could provide more selectivity and better understanding for the samples probed in comparison with XAS.

RIXS on NiF₂ and two other covalent Ni complexes was also performed. These measurements used an excitation energy of 70 eV [Figs. 3(d)–3(f)]. Although NiF₂ also contains high-spin Ni(II), its RIXS feature shows d - d transitions at 0.8 and 1.5 eV, different from NiO. There might be a weak peak(s) at ~ 2 eV. The difference between NiO and NiF₂ RIXS is not unexpected, because the d - d structures can be different for complexes with a similar ionicity and even a similar geometry. The difference between the L_3 XAS absorption centroids for NiO and NiF₂ indicates that the two have different $3d$ energy levels (and thus d - d structures).

The covalent complex [Ni(II)(tfd)₂][−] has almost no RIXS feature (Fig. 3e). [Ni(III)(tfd)₂][−] is also a dilute and covalent complex, but it shows weak features at 0.5/0.7 and 1.3 eV. The weak but detectable spectral features of $M_{2,3}$ -edge RIXS on this covalent complex provide hope that future RIXS studies

could be extended to more biologically relevant complexes if beamlines and spectrometers continue to improve. It also motivates the exploration of more sensitive and more effective detection methods.

3.4. X-ray detectors below 100 eV

M -edge XAS and RIXS spectroscopies on biological or dilute samples, whose metal content is often 0.1% by weight or less, are currently hindered by the limited detector technologies in the energy region below 100 eV. Non-dispersive channeltron or photocurrent measurements suffer from a large background that obscures low-level signals. For example, the TEY measurements have a practical detection limit of 5% of Ni(OH)₂ in this study, which corresponds to a Ni concentration of $\sim 3\%$. Grating spectrometers also require high metal concentrations because of their very low optical throughput.

Semiconductor X-ray detectors have an energy resolution of about 50–150 eV, and therefore are very good at resolving K -edges (4–10 keV, $\Delta E/E \simeq 0.01$) for all $3d$ metals and L -edges for heavier $3d$ metals (*e.g.* Fe–Zn, 700–1000 eV, $\Delta E/E \simeq 0.1$) from the background signals (C, N, O K -edges at 288–512 eV). These detectors have been used for many years in K -edge and L -edge XAS measurements on various biological samples (Wang *et al.*, 2000; George *et al.*, 2009). However, for measurements at <100 eV, better energy resolution is required.

Superconducting tunnel junctions (STJs) are electronic devices consisting of two superconductors separated by a very thin layer of insulating material. Current passes through the junction *via* the quantum-mechanical process of tunneling. STJ X-ray detectors exploit the small energy gap in superconducting materials (~ 1 meV *versus* ~ 1 eV for Si or Ge) to achieve orders of magnitude higher energy resolution than conventional semiconductor detectors (le Grand *et al.*, 1998; Verhoeve *et al.*, 2002; Friedrich, 2006). STJs exhibit an

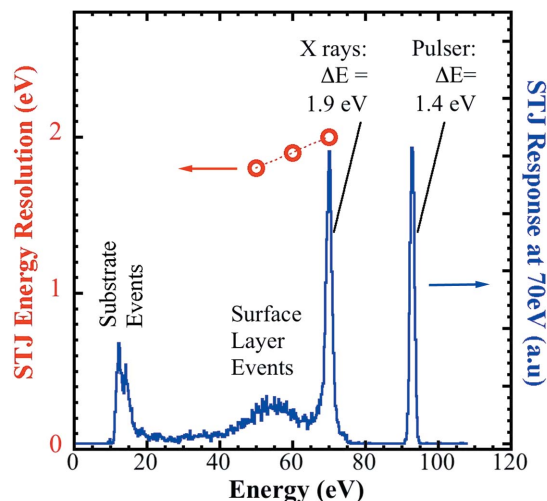


Figure 4

Spectral response of a STJ X-ray detector (blue) at an excitation energy of 70 eV with 1.9 eV FWHM. The red open circles are the energy resolution at energies of 50, 60 and 70 eV.

exceptional performance in the region below 100 eV, although they were not used in measuring the complexes in this study. For example, our STJ detector has an energy resolution of 1.9 eV and a maximum count rate of ~ 10000 counts s^{-1} per detector pixel at energies below 100 eV (Fig. 4) (Friedrich *et al.*, 1999; Drury & Friedrich, 2005). Its single-photon detection sensitivity reduces the detection threshold, while its high energy resolution allows unwanted background counts to be rejected to further improve the detection limit.

In practice, the achievable detection limit will also depend on the fluorescence yield, the STJ array size, and some practical issues such as the transmission of the IR-blocking windows (Drury & Friedrich, 2005). X-ray spectrometers with about 100 STJ detector pixels are currently being developed, which should make it feasible to measure *M*-edge XAS to resolve the 3*d* metal electronic structure in biological systems.

4. Conclusions

M-edge XAS or RIXS can provide complementary information to *K*- and *L*-edge spectroscopies. $M_{2,3}$ -edge XAS on several Co, Ni and Cu complexes have been measured and their spectral information analyzed and discussed. For example, *M*-edge XAS has revealed a chemical shift of 0.8 eV between LiNiO₂ and NiO, which indicates that LiNiO₂ has a Ni oxidation state higher than Ni(II). The covalence in Ni halides has also been examined.

In addition, $M_{2,3}$ -edge RIXS-observed *d*-*d* transitions on several ionic and covalent Ni complexes {*e.g.* NiO, NiF₂, [Ni(II)(tfd)₂][−] and [Ni(III)(tfd)₂][−]} were measured and analyzed. NiO RIXS features are consistent with the earlier *M*-edge and *K*-edge RIXS reports (Chiuzbaian *et al.*, 2005; van Veenendaal *et al.*, 2011). Successful RIXS observations on the covalent [Ni(III)(tfd)₂][−] complex provide motivation to pursue more complicated 3*d* metal complexes in the future.

The above $M_{2,3}$ -edge XAS and RIXS work motivates the exploration of more sensitive and more effective detection methods to improve the detectability on dilute samples. For this purpose a high-sensitivity and high-resolution STJ X-ray detector was evaluated in this study for possible applications below 100 eV.

This research is part of the Advanced Biological Experimental X-ray spectroscopy (ABEX) program, which is supported by the US Department of Energy, Office of Biological and Environmental Research. The research is also supported by the National Institutes of Health (GM-65440). The Advanced Light Source is supported by the Department of Energy, Office of Basic Energy Sciences. All the LBNL work is under the DOE/LBNL contract DE-AC02-05CH11231. Part of this work was performed under the auspices of the US DOE by Lawrence Livermore National Laboratory under Contract DE-AC52-07NA27344. We also thank Dr Carlos Malendres (Argonne National Laboratory), and Dr Kung Wang (ExxonMobil Research Co.) for providing the LiNiO₂ and two Ni dithiolene samples. AB had financial

support by the Swiss National Science Foundation (project number 200021-132126).

References

- Branchard, P. E., Grosvenor, A. P., Cavell, R. G. & Mar, A. (2008). *Chem. Mater.* **20**, 7081–7088.
- Braun, A., Wang, H., Shim, J., Lee, S. S. & Cairns, E. J. (2007). *J. Power Sources*, **170**, 173–178.
- Chen, H. & Harding, J. H. (2012). *Phys. Rev. B*, **85**, 115127.
- Chiuzbaian, S. G., Ghiringhelli, G., Dallera, C., Grioni, M., Amann, P., Wang, X., Braicovich, L. & Patthey, L. (2005). *Phys. Rev. Lett.* **95**, 197402.
- Chiuzbaian, S. G., Schmitt, T., Matsubara, M., Kotani, A., Ghiringhelli, G., Dallera, C., Tagliaferri, A., Braicovich, L., Scagnoli, V., Brookes, N. B., Staub, U. & Patthey, L. (2008). *Phys. Rev. B*, **78**, 245102.
- Cramer, S. P., Wang, H.-X., Bryant, C., LeGros, M., Horne, C., Patil, D., Ralston, C. & Wang, X. (1998). *ACS Ser.* **692**, 154–178.
- CXRO (2000). *X-ray Data Booklet*, http://xdb.lbl.gov/Section1/Sec_1-1.html.
- Drury, O. B. & Friedrich, S. (2005). *IEEE Trans. Appl. Supercond.* **15**, 613–617.
- Elp, J. van, Eskes, H., Kuiper, P. & Sawatzky, G. (1992). *Phys. Rev. B*, **45**, 1612–1622.
- Friedrich, S. (2006). *J. Synchrotron Rad.* **13**, 159–171.
- Friedrich, S., le Grand, J. B., Hiller, L. J., Kipp, J., Frank, M., Labov, S. E., Cramer, S. P. & Barfknecht, A. T. (1999). *IEEE Trans. Appl. Supercond.* **9**, 3330–3333.
- George, S. J., Drury, O. B., Fu, J., Friedrich, S., Doonan, C. J., George, G. N., White, J. M., Young, C. G. & Cramer, S. P. (2009). *J. Inorg. Biochem.* **103**, 157–167.
- Grand, J. B. le, Mears, C. A., Hiller, L. J., Frank, M., Labov, S. E., Netel, H., Chow, D., Friedrich, S., Lindeman, M. A. & Barfknecht, A. T. (1998). *Appl. Phys. Lett.* **73**, 1295.
- Gunnelin, K., Glans, P., Rubensson, J., S  the, C., Nordgren, J., Li, Y., Gel'mukhanov, F. &   gren, H. (1999). *Phys. Rev. Lett.* **83**, 1315–1318.
- Guo, J. H., Luo, Y., Augustsson, A., Kashtanov, S., Rubensson, J. E., Shuh, D. K., Agren, H. & Nordgren, J. (2003). *Phys. Rev. Lett.* **91**, 157401.
- Guo, X., Greenbaum, S., Ronci, F. & Scrosati, B. (2004). *Solid State Ion.* **168**, 37–49.
- Koide, T., Shidara, T., Fukutani, H., Yamaguchi, K., Fujimori, A. & Kimura, S. (1991). *Phys. Rev. B*, **44**, 4697–4700.
- Kuiper, P., Guo, J., S  the, C., Duda, L., Nordgren, J., Pothuizen, J., de Groot, F. & Sawatzky, G. (1998). *Phys. Rev. Lett.* **80**, 5204–5207.
- Kuiper, P., Kruizinga, G., Ghijsen, J., Sawatzky, G. A. & Verweij, H. (1989). *Phys. Rev. Lett.* **62**, 221–224.
- Laan, G. van der & Kirkman, I. W. (1992). *J. Phys. Condens. Matter*, **4**, 4189–4204.
- Lancaster, J. R. (1988). *The Bioinorganic Chemistry of Nickel*. New York: VCH.
- Lee, S. K., Eng, P. J., Mao, H.-K., Meng, Y. & Shu, J. (2007). *Phys. Rev. Lett.* **98**, 105502.
- Mansour, A. N. & Melendres, C. A. (1997). *J Phys IV*, **7**, 1171–1172.
- Montoro, L., Abbate, M., Almeida, E. & Rosolen, J. (1999). *Chem. Phys. Lett.* **309**, 14–18.
- Ohzuku, T. & Makimura, Y. (2006). *Res. Chem. Intermed.* **32**, 507–521.
- Okada, K. & Kotani, A. (1992). *J. Phys. Soc. Jpn.* **61**, 449–453.
- Pickering, I. J., George, G. N., Lewandowski, J. T. & Jacobson, A. J. (1993). *J. Am. Chem. Soc.* **115**, 4137–4144.
- Rao, M. M., Liebenow, C., Jayalakshmi, M., Wulff, H., Guth, U. & Scholz, F. (2001). *J. Solid State Electrochem.* **5**, 348–354.
- Rougier, A., Delmas, C. & Chadwick, A. (1995). *Solid State Commun.* **94**, 123–127.

- Sonntag, B. (1974). *Phys. Rev. B*, **9**, 3601–3602.
- Steiner, P., Zimmermann, R., Reinert, F., Engel, T. & Hufner, S. (1996). *Z. Phys. B*, **99**, 479–490.
- Stohr, J. (1992). *NEXAFS Spectroscopy*. New York: Springer-Verlag.
- Veenendaal, M. van, Liu, X., Carpenter, M. H. & Cramer, S. P. (2011). *Phys. Rev. B*, **83**, 045101.
- Verhoeve, P., Rando, N., Peacock, A., Martin, D. & den Hartog, R. (2002). *Opt. Eng.* **41**, 1170–1184.
- Waddill, G. D., Cummins, T. R., Moore, D. P., Long, G. J. & Buschow, K. H. J. (1998). *Abstr. Pap. Am. Chem. Soc.* **215**, U797.
- Wang, H., Ge, P., Riordan, C. G., Brooker, S., Woomer, C. G., Collins, T., Melendres, C. A., Graudejus, O., Bartlett, N. & Cramer, S. P. (1998). *J. Phys. Chem. B*, **102**, 8343–8346.
- Wang, H., Ralston, C. Y., Patil, D. S., Jones, R. M., Gu, W., Verhagen, M., Adams, M., Ge, P., Riordan, C., Marganian, C. A., Mascharak, P., Kovacs, J., Miller, C. G., Collins, T. J., Brooker, S., Croucher, P. D., Wang, K., Stiefel, E. I. & Cramer, S. P. (2000). *J. Am. Chem. Soc.* **122**, 10544–10552.
- Young, A. T., Martynov, V. & Padmore, H. A. (1999). *J. Electron Spectrosc. Relat. Phenom.* **101**, 885–889.